

# Harnessing Extreme Internal Damping in Polyrotaxane-Incorporated Liquid Crystal Elastomers for Pressure-Sensitive Adhesives

Subi Choi, Hongye Guo, Bitgaram Kim, Ji-Hun Seo,\* Eugene M. Terentjev, Mohand O. Saed,\* and Suk-kyun Ahn\*

Liquid crystal elastomers (LCEs) exhibit extraordinary energy dissipation due to their unique viscoelastic response, resulting from the rotation of mesogens under mechanical stress. While recent studies demonstrate the LCE-based pressure-sensitive adhesives (PSAs) by exploiting the enhanced damping, all previous studies have focused on LCEs with covalent crosslinks. Here, a new class of PSAs is developed by integrating movable polyrotaxane crosslinkers into an LCE matrix (PRx-LCEs). Dynamic viscoelastic measurements reveal that PRx-LCE exhibits a remarkably high energy dissipation, as indicated by a large  $\tan \delta$ . Interestingly, the secondary  $\tan \delta$  peak associated with LCE damping is more pronounced than the primary peak of the glass transition. The exceptional energy dissipation in PRx-LCE results in superior adhesion strength ( $\approx 1864 \text{ N m}^{-1}$ ), which is 3.5 times higher than conventional LCEs and 13 times higher than commercial PSAs in the peel test. Additionally, PRx-LCEs demonstrate thermally reversible adhesion, enabling clean removal at elevated temperatures. Furthermore, the sliding effect in PRx-LCE enhances both deformability and stress relaxation under load, resulting in deeper indentation, and superior adhesion during the probe tack test. The combination of LCE and slidable crosslinks provides robust and switchable adhesion, making them promising for applications in biomedical engineering, display, and semiconductor industries.

A key property of LCEs for energy absorption applications is due to the local mesogen rotation during deformation, characterized by a high loss factor (occurring above the glass transition,  $T_g$ ) in dynamic mechanical measurements.<sup>[16]</sup> This unique dynamic feature of LCEs suggests a great potential for high-damping applications.<sup>[17,18]</sup>

Recently, several studies have exploited the unique energy dissipation of LCEs to develop high-performance pressure-sensitive adhesives (PSAs), although the direct correlation between energy dissipation and adhesion remains largely empirical.<sup>[19–24]</sup> For instance, Terentjev and coworkers were able to correlate the dynamic adhesion and viscoelastic behavior of LCEs, demonstrating switchable adhesion through a nematic-to-isotropic transition ( $T_{ni}$ ).<sup>[20]</sup> This correlation between  $\tan \delta$  and adhesive energy follows from assessing the adhesion strength in relation to crosslinking density, orientational genesis, and surface roughness.<sup>[21]</sup> They also explored various adhesion characteristics of LCEs using 90° peel, lap shear, and probe tack tests.<sup>[22]</sup> More recently, Cai and coworkers reported the details of

the rate-dependence of LCE adhesion using the 180° peel tests.<sup>[23]</sup> While most adhesion studies have focused on polydomain LCEs, the White research group investigated monodomain well-aligned LCEs, highlighting their directional adhesion under nonlinear deformation.<sup>[24]</sup> Despite the growing interest in LCE-based PSAs, all previous work has mainly focused on LCEs with covalent or fixed crosslinks.

A new strategy for enhancing the energy dissipation of elastomers is the incorporation of movable crosslinks. Polyrotaxane

## 1. Introduction

Liquid crystal elastomers (LCEs) which combine the anisotropic and stimuli-responsive properties of liquid crystals with the elasticity of the polymer networks are renowned for their use in shape-changing applications such as actuators,<sup>[1–6]</sup> soft robotics,<sup>[7,8]</sup> artificial muscles,<sup>[9,10]</sup> and biomedical devices.<sup>[11]</sup> However, recent studies have also highlighted their potential in other compelling applications, including energy dissipation materials,<sup>[12,13]</sup> shock absorbers,<sup>[14]</sup> and vibration dampers.<sup>[15]</sup>

S. Choi, S.-k. Ahn  
School of Chemical Engineering  
Pusan National University  
Busan 46241, Republic of Korea  
E-mail: skahn@pusan.ac.kr

The ORCID identification number(s) for the author(s) of this article can be found under <https://doi.org/10.1002/adfm.202413824>

DOI: 10.1002/adfm.202413824

H. Guo, E. M. Terentjev, M. O. Saed  
Cavendish Laboratory  
University of Cambridge  
Cambridge CB3 0HE, UK  
E-mail: mos29@cam.ac.uk

B. Kim, J.-H. Seo  
Department of Materials Science and Engineering  
Korea University  
Seoul 02841, Republic of Korea  
E-mail: seojh79@korea.ac.kr

(PRx) is well-known for its sliding effect, which enhances the energy dissipation and toughness of elastomers. The sliding effect, also called the “molecular pulley effect”, arises from the movement of the cyclodextrin rings along the polymer axes, leading to stress-relaxation behavior and increased stretchability. The sliding effect can be observed between the glassy and rubbery states when the cyclic rings gain sufficient thermal energy to actively move, resulting in an additional  $\tan \delta$  peak.<sup>[25]</sup> This stress-relaxation behavior of PRx can also enhance adhesion strength. Recent studies have demonstrated that acrylic PSAs incorporating slidable crosslinks exhibit exceptional adhesion and stretchability.<sup>[26]</sup> Additionally, PSAs based on poly(lipoic acid) incorporating PRx crosslinkers can withstand significant weights due to their enhanced stress dissipation.<sup>[27]</sup> Consequently, we hypothesized that introducing PRx crosslinkers into LCEs would add extra movable moieties in addition to the intrinsic mesogenic rotation of LCEs, thereby maximizing the damping and adhesion properties.

In this study, we developed a new class of high-performance PSAs based on LCEs comprising polyrotaxane crosslinkers (PRx-LCEs). PRx-LCE with an optimal PRx content shows two distinct  $\tan \delta$  peaks in dynamic viscoelastic measurements: a low-temperature peak associated with the segmental motion of LCE, and a high-temperature peak related to the rotation of mesogens. Notably, the secondary  $\tan \delta$  peak from the rotational dissipation of LCE is more pronounced in PRx-LCE compared to conventional LCE, due to the additional sliding effect of polyrotaxane adding mobility to fluctuating mesogenic groups. This pronounced secondary  $\tan \delta$  peak, greater than the primary peak associated with the  $T_g$ , is extremely unusual in conventional polymers. Owing to its superior damping, the PRx-LCE-based PSA also demonstrated higher adhesion performance than both conventional LCE adhesives and commercial PSAs, as confirmed by the 180° peel and probe tack tests.

## 2. Results and Discussion

### 2.1. Synthesis and Viscoelastic Properties of PSAs

All LCE samples were prepared using a two-step synthesis process (chain extension followed by photopolymerization) according to our previously reported protocol (Figure S1, Supporting Information).<sup>[28]</sup> Briefly, a homogeneous LC mixture consisting of diacrylate-functionalized reactive mesogen (RM82), *n*-butylamine (*n*-BA) chain-extender, and a photoinitiator (I-369) was heated in a convection oven at 80 °C for 21 h, resulting in oligomerization through the aza-Michael addition reaction. The resulting LC oligomer was bar-coated onto 70  $\mu\text{m}$  PET backing films to the desired thickness, followed by photopolymerization at room temperature to yield LCE film. For PRx-LCE, a multiacrylate functionalized PRx crosslinker was thoroughly mixed with the LC oligomer using chloroform as solvent prior to bar-coating. As a control, an isotropic film comprising the same weight percentage of PRx crosslinker was also prepared using bisphenol A ethoxylate diacrylate (BADA) as a non-LC monomer. This setup allows for a comparison of the viscoelastic properties and adhesion performance among PRx-LCE which consists of an anisotropic matrix with movable crosslinks, a conventional LCE with fixed crosslinks, and PRx-BADA, which consists of an

isotropic matrix with movable crosslinks (Figure 1a). The fabrication process of adhesive tapes through bar-coating and photocrosslinking is illustrated in Figure 1b and Video S1 (Supporting Information).

The viscoelastic properties of LCEs can provide insights into their adhesive properties, with a higher  $\tan \delta$  (i.e., greater energy dissipation) suggesting stronger adhesion.<sup>[20,24]</sup> The viscoelastic properties of LCE, PRx-LCE, and PRx-BADA were investigated by dynamic mechanical analysis (DMA) from a temperature ramp in tensile mode, and the resulting storage modulus and  $\tan \delta$  curves are shown in Figure 2a,b, respectively. The crosslink density ( $\nu_e$ ) of each sample was estimated based on the rubbery modulus according to Equation (1).

$$\nu_e = \frac{E'}{3RT} \quad (1)$$

where  $E'$  is the storage modulus at 120 °C,  $R$  is the gas constant, and  $T$  is the temperature (in Kelvin). The crosslinking densities of LCE, PRx-LCE, and PRx-BADA were determined to be  $1.6 \times 10^{-5}$ ,  $0.7 \times 10^{-5}$ , and  $8.5 \times 10^{-5} \text{ mol cm}^{-3}$ , respectively.

From the  $\tan \delta$  curves,  $T_g$  of all samples was observed at  $\approx 15$  °C, but  $T_{ni}$  of LCEs was not apparent due to its weak and broad characteristics as well as the networked structure.<sup>[29,30]</sup> Note that  $T_{ni}$  ( $\approx 110$  °C) of LCE samples could be better identified by differential scanning calorimetry (DSC) analyses (Figure S2, Supporting Information). Interestingly, both LCE and PRx-LCE exhibited distinct secondary  $\tan \delta$  peaks at  $\approx 60$  °C, associated with the rotational dissipative loss.<sup>[18,20,28]</sup> More interestingly, the secondary peak of PRx-LCE was even more pronounced than the corresponding primary glass-transition peak ( $T_g$ ). In most polymers, the  $\tan \delta$  peak exhibits its maximum at  $T_g$ , where the segmental motion starts during the transition from the glassy to rubbery state. Therefore, the greater secondary  $\tan \delta$  peak observed in the nematic phase of PRx-LCE is extremely unusual. This secondary peak was consistently observed in the  $\tan \delta$  curves throughout three heating cycles, as shown in Figure S3 (Supporting Information). In contrast, the secondary peak in  $\tan \delta$  curve was not observed in PRx-BADA (Figure 2b), suggesting that the rotational motion of mesogens is primarily responsible for inducing the secondary peak. Apparently, the further enhanced mechanical dissipation of PRx-LCE is attributed to the sliding motion of the movable polyrotaxane crosslinkers, which do not significantly interfere with the movement of mesogens, unlike traditional covalently crosslinked LCEs.

To investigate the effect of sliding motion on internal damping, we conducted several control experiments. First, we examined the impact of LC monomers and crosslinking density in LCEs on internal damping. We used RM82 (six methylene spacers, S6) and RM257 (three methylene spacers, S3) as LC monomers, while varying the crosslinking density by adjusting the LC monomer to chain extender ratio ( $m:1$ , with  $m = 1.01, 1.1$ , and  $1.2$ ). PRx content and the number of cyclodextrin (CD) rings were fixed at 0.5 wt.% and  $n = 50$ . PRx-LCE with a longer spacer (S6) exhibited a broader  $\tan \delta$  peak over a wider temperature range (Figure S4a, Supporting Information), while lower crosslinking densities ( $m = 1.01$  and  $1.1$ ) showed distinct secondary  $\tan \delta$  peaks (Figure S4b, Supporting Information). Although PRx-LCE ( $m = 1.01$ ) had strong damping, its

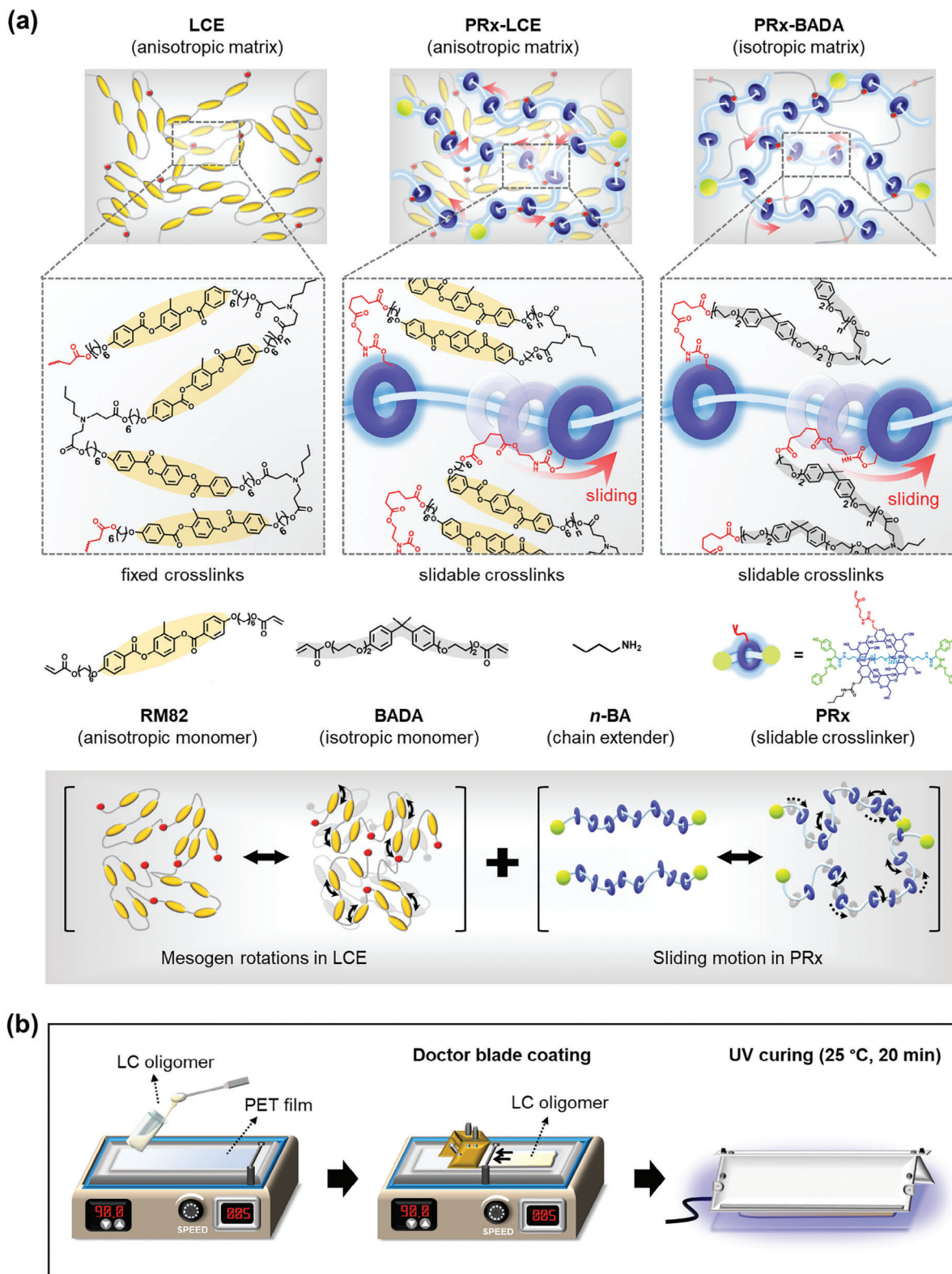


**Figure 1.** a) Schematic of the three distinct samples used in this study highlighting their differences in molecular structures: LCE, PRx-LCE, and PRx-BADA (top), and the mesogen rotation in LCE and sliding motion of PRx (bottom), and b) Fabrication process of the pressure sensitive adhesive (PSA).

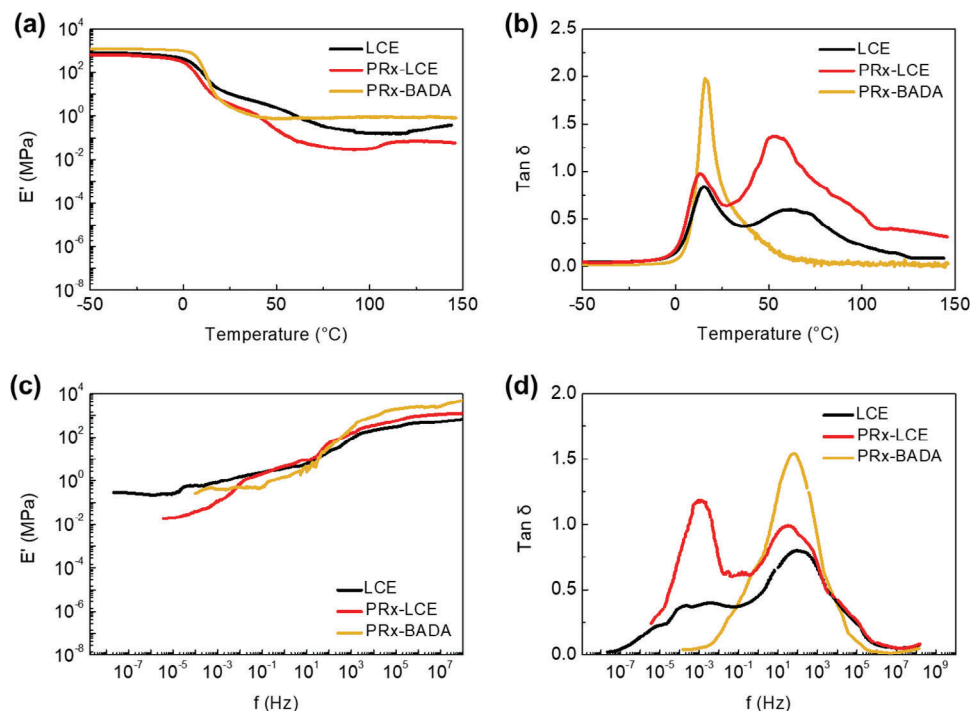


**Figure 2.** a) Storage modulus and b)  $\tan \delta$  curves of LCE, PRx-LCE, and PRx-BADA during temperature ramp in DMA. Master curves of the c) storage modulus and d)  $\tan \delta$  against the shifted frequency of LCE, PRx-LCE, and PRx-BADA, obtained by time-temperature superposition from frequency sweep at various temperatures and frequencies.

mechanical strength was insufficient to measure adhesion properties. Thus, PRx-LCE with 1) a longer spacer length (S6) and 2) an intermediate crosslinking density ( $m = 1.1$ ) was selected for optimal balance between damping and mechanical stability. Second, LCE incorporates a 0.5 wt.% PRx crosslinker exhibited the highest secondary peak (Figure S5a, Supporting Information). Interestingly, the mechanical dissipation of PRx-LCE increased with increasing PRx content. However, an excessive PRx content (1–2 wt.%) resulted in inefficient sliding motion due to agglomeration.<sup>[28]</sup> Therefore, the content of the PRx crosslinker was set at 0.5 wt.% in all remaining experiments. Third, a higher number of cyclodextrin (CD) ( $n = 50$ ) effectively increased the peak magnitude compared to a lower number of CD ( $n = 30$ ) (Figure S5b, Supporting Information). A higher number of CDs causes a greater number of slidable crosslinks, consequently increasing viscoelastic relaxation. According to previous studies, PRx exhibits additional viscoelastic relaxation at intermediate temperatures ( $\approx 25$ – $150$  °C) due to the sliding motion of the CD rings.<sup>[31,32]</sup> Additionally, an increase in PRx content can lead to an increase in peak magnitude.<sup>[33]</sup> Consequently, our findings indicate that 1) an optimized PRx content and the number of CD rings enhance the loss peak magnitude; 2) this increase originates from additional viscoelastic relaxation through the molecular motion of the CD rings; and 3) these effects are specifically observed in an anisotropic matrix with nematic order. Therefore, the superior internal damping in PRx-LCE results from the synergistic interaction between mesogen rotation and the sliding motion of PRx. Hence, we suggest that slidable crosslinks play a crucial role in enhancing the energy dissipation of LCEs.

## 2.2. Master Curves

The complete viscoelastic behavior of LCEs was investigated by constructing a Master Curve using the time-temperature superposition (TTS) principle, which provides insights into the adhesion performance over extensive timescales. Frequency sweep test was conducted at various temperatures, and the frequency was shifted to achieve the overlap of curves at different temperatures to construct a Master Curve of the storage modulus and  $\tan \delta$ .<sup>[23]</sup> The multiplicative factor by which the frequency was shifted (the so-called shift factor  $aT$ ) is equal to 1 at a reference temperature ( $T_{ref} = 20$  °C). The shift factor and fitting curves, based on the Williams–Landel–Ferry (WLF) equation at different temperatures,<sup>[34,35]</sup> are presented in Figure S6 (Supporting Information).

Figure 2c shows the master curves of the storage modulus of LCE, PRx-LCE, and PRx-BADA. Notably, above  $T_{ni}$ , the TTS principle does not apply to the storage modulus. Indeed, the storage modulus increased in the isotropic phase above  $T_{ni}$  due to entropic rubber elasticity (Figure S7, Supporting Information).<sup>[15,35]</sup> However, below  $T_{ni}$ , the storage modulus observed in the master curves closely aligns with the results from the temperature-ramp experiments (Figure 2a). The master curves of the storage modulus of PRx-BADA also aligned well with the temperature-ramp results (Figure 2a). However, constructing reliable master curves at low frequencies was restricted by the limited deformability of PRx-BADA at elevated temperatures (Figures S9 and S10, Supporting Information).

The master curves of  $\tan \delta$  of LCE, PRx-LCE, and PRx-BADA are shown in Figure 2d, demonstrating a good agree-



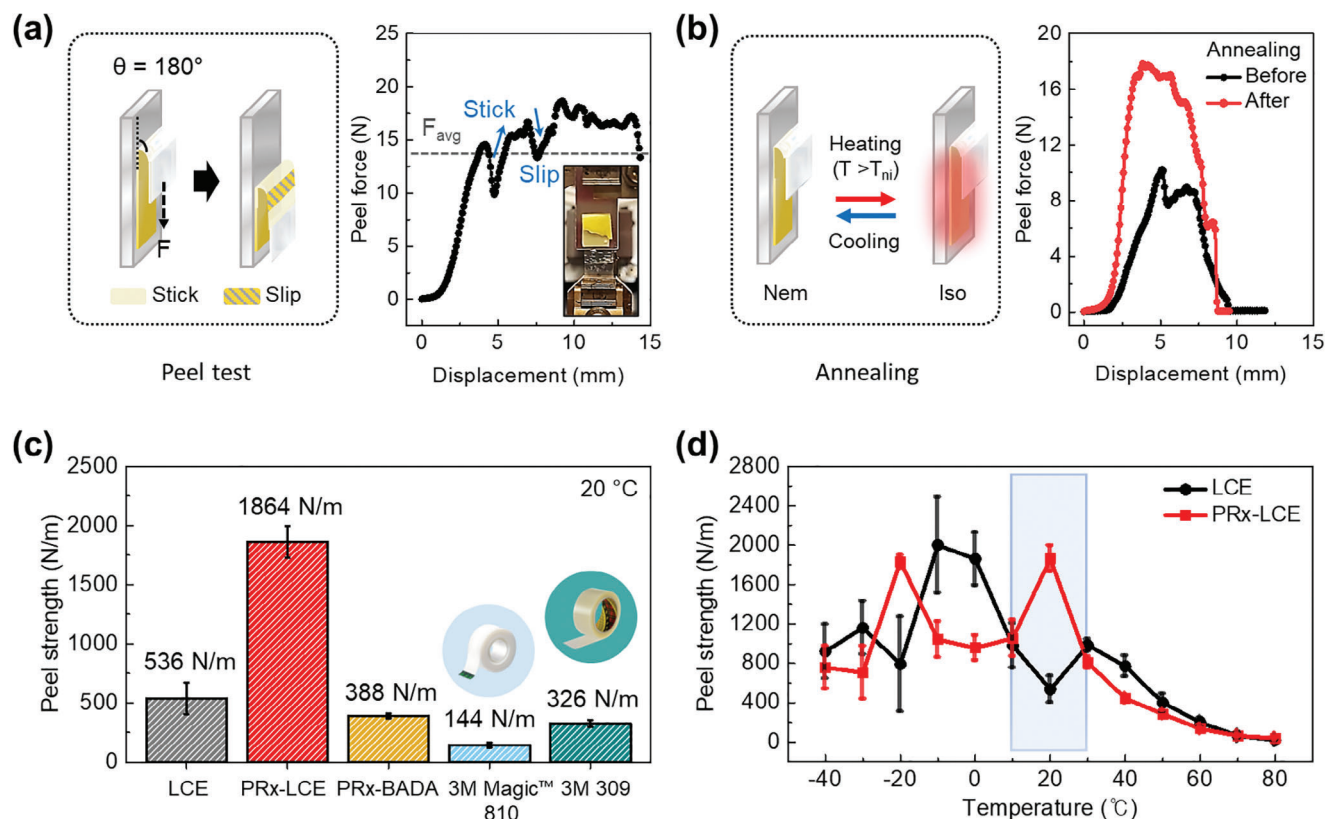


**Figure 3.** a) Peel force–displacement curve obtained from a 180° peel test at a peel rate of 100 mm min<sup>−1</sup>, indicating a stick–slip behavior. b) Peel force–displacement curve before and after thermal annealing. c) Peel strength of LCE, PRx-LCE, PRx-BADA, and commercial 3M tapes measured at 20 °C. d) Peel strength of LCE and PRx-LCE measured at various temperatures.

ment with the results of the temperature ramp (Figure 2b). The frequency sweep results at each different temperature are provided in Figures S8 and S9 (Supporting Information). Generally, a high  $\tan \delta$  (>1) represents a greater adhesive energy, as it correlates with increased energy dissipation during the debonding process.<sup>[36,37]</sup> Notably, PRx-LCE exhibits a higher  $\tan \delta$  (>1) within the 10<sup>−4</sup>–10<sup>3</sup> Hz frequency range, whereas LCE shows a much lower  $\tan \delta$  (<1). These findings suggest that PRx-LCE can maintain its adhesion strength at both ultra-low and ultra-high peel rates (or equivalently, frequencies of the dynamic response), making it advantageous for applications requiring reliable adhesion or damping across a wide range of frequencies and temperatures.

### 2.3. Peel Strength

As previously discussed, the temperature- and time-dependent viscoelastic properties are closely related to adhesion strength. Given the unique viscoelastic characteristics of PRx-LCE, we anticipate superior adhesive performance compared to conventional LCE. To assess the adhesion strength of PSAs, a 180° peel test was performed at 20 °C. During the peel test, the adhesives were affixed to a stainless-steel substrate and subjected to constant-rate peeling using DMA (Video S2, Supporting Information). Figure 3a displays the displacement versus peel force

curve, highlighting stick–slip behavior. The average peel force ( $F_{avg}$ ) was computed from the curve as the mean value between the initiation force (minimum value) and the arrest force (maximum value).<sup>[38]</sup> Figure 3b displays the peel forces before and after annealing. Annealing enhanced the adhesion force by promoting the gradual stress relaxation of polydomain LCEs, which is consistent with recent studies on LCE adhesives.<sup>[22]</sup> Therefore, all peel tests were conducted following annealing to an isotropic state and subsequent rapid cooling to room temperature (Figure S11, Supporting Information).

Figure 3c shows the peel strength of LCE, PRx-LCE, PRx-BADA, and two types of commercial 3M tapes (3M 810 and 3M 309) at 20 °C. The peel force was normalized to the width of each sample to provide standardized values of “work of adhesion”, allowing for comparisons between the different adhesive systems. The PRx-LCE adhesive exhibits a peel strength ( $\approx 1864$  N m<sup>−1</sup>) that is 3.5 times higher than that of LCE ( $\approx 536$  N m<sup>−1</sup>). Additionally, PRx-LCE shows a peel strength 13 times higher than that of 3M 810 ( $\approx 144$  N m<sup>−1</sup>) and 5.7 times higher than 3M 309 ( $\approx 326$  N m<sup>−1</sup>). In contrast, PRx-BADA adhesive demonstrates a lower peel strength ( $\approx 388$  N m<sup>−1</sup>) than both LCE and PRx-LCE; a detailed analysis of this lower peel strength will be discussed later (Figure S12, Supporting Information). To evaluate the temperature-dependent adhesion performance of PSAs, peel tests were conducted at various temperatures (Figure 3d). Both samples displayed two distinct peaks in peel strength: one

occurring at lower temperatures ( $-30$  to  $10$  °C) and another at higher temperatures ( $10$  to  $50$  °C). Specifically, PRx-LCE exhibited peak peel strengths of  $\approx 1833$  N m $^{-1}$  at  $-20$  °C and  $\approx 1864$  N m $^{-1}$  at  $20$  °C. In comparison, LCE showed a maximum peel strength of  $\approx 2000$  N m $^{-1}$  at  $-10$  °C, which decreased to  $\approx 984$  N m $^{-1}$  at  $30$  °C. The observed maximum peaks in peel strength are correlated with  $T_g$  and nematic dissipation identified by the  $\tan \delta$  curves, although the peak temperatures do not entirely align with those observed in viscoelastic measurements (Figure 2b).

The discrepancy between the peaks in the  $\tan \delta$  and peel strength curves is associated with the rate-dependent characteristics of viscoelastic behavior and peel strength during each test.<sup>[20,23]</sup> Specifically, the oscillating frequency used during DMA measurement ( $1$  Hz) does not directly correlate with the peeling rate ( $100$  mm min $^{-1}$ ) during the peel test, which may result in the peak temperatures, appearing at different values in each test. Nevertheless, the key trends remain consistent. Notably, the two distinct transitions identified in the  $\tan \delta$  curves, corresponding to the  $T_g$  and internal damping, are reflected in the temperature-dependent peel strength. Consequently, the strong adhesion of PRx-LCE at  $20$  °C is attributed to its pronounced rotational dissipation, enhanced by PRx sliding.

Additionally, both samples displayed a decrease in peel strength to below  $\approx 0.5$  N ( $50$  N m $^{-1}$ ) when heated from  $20$  °C (nematic phase) to  $100$  °C (near isotropic phase), which agrees with the  $\tan \delta$  results (Figure S13, Supporting Information). Consistent with other literature,<sup>[20–22]</sup> the contact angles of all samples were found to be similar at nematic and isotropic temperatures, indicating that the adhesion of LCEs is mainly governed by the viscoelastic behavior rather than by interfacial energy (Figure S14, Supporting Information). The reusability of the PRx-LCE adhesive was assessed, demonstrating nearly consistent peel strength over  $\approx 13$  tests at  $20$  °C, after which the PET film failed (Figure S15, Supporting Information). The excellent reusability after a peel test is attributed to the capability of PRx-LCE to restore its original form through annealing at  $150$  °C ( $T > T_{ni}$ ). The above findings highlight PRx-LCE as a promising candidate for switchable PSAs with demonstrating reliable adhesion performance across a broad range of temperatures.

To visualize the peel strength, the LCE and PRx-LCE adhesives were affixed to a glass cell, subjected to thermal annealing, and then monitored under a sustained load at  $25$  °C. As shown in Figure 4a,b, the LCE adhesive sustained a load of  $500$  g for  $20$  min, but detached at  $1$  kg (Video S3, Supporting Information). In contrast, the PRx-LCE adhesive could hold  $500$  g for  $1$  h,  $1$  kg for  $2$  min, and  $2$  kg for  $15$  s. The maximum holding weights ( $500$  g for LCE and  $2$  kg for PRx-LCE) are in good agreement with the peel test results ( $5$  N for LCE and  $18$  N for PRx-LCE) (Figure 3c). The higher peel strength of PRx-LCE is attributed to its enhanced internal damping. The adhesion of PRx-LCE can be eliminated by heating above  $T_{ni}$  with a heat gun at  $150$  °C for  $5$  s, resulting in removal of the load (Figure 4c; Video S4, Supporting Information). The loss of adhesion at elevated temperatures (in the isotropic phase of the elastomers) was due to the reduced peel strength of PRx-LCE under these conditions (Figure 3d). Upon reattachment, the adhesion strength of PRx-LCE was restored by annealing above  $T_{ni}$ , allowing it to support the same load. The adhesion could then be eliminated again by heating, demonstrating

its reversible and switchable adhesion (Figure S16, Supporting Information).

In addition to robust adhesion, the clean removal of PSA without leaving residues is crucial for various applications such as medical bandages,<sup>[39]</sup> label tapes,<sup>[40]</sup> and circuit boards.<sup>[41]</sup> Therefore, we also evaluated the adhesive residue after detaching each PSA from glass substrates. For this purpose, LCE and PRx-LCE adhesives, along with commercial 3M tape, were applied to glass substrates and peeled at  $90$  °C (near  $T_{ni}$ ) using DMA at a constant rate. After peeling, the glass substrate surfaces were analyzed using a laser-scanning confocal microscope. Both LCE and PRx-LCE adhesives showed minimal residues, as evidenced by 2D optical images (Figure 4d) and height profiles (Figure 4e), suggesting adhesive failure at elevated temperatures. These findings correspond with the significant drop in peel strength observed at  $T_{ni}$  for LCE and PRx-LCE adhesives (Figure 3d). In contrast, the commercial 3M tape exhibited cohesive failure, leaving substantial residue upon detachment.

## 2.4. Probe Tack Adhesion

The surface tackiness of our PSAs was evaluated using a probe tack test under a constant compressive load of  $0.5$  N. Figure 5a shows a schematic of this experiment along with a general plot of the adhesion force over contact time. The adhesion force ( $F_a$ ) is determined from the peak of the force–displacement (or the force–time) curve, whereas the work of adhesion ( $W_a$ ) is determined from the area under the stress–displacement curve. Figure 5b,c shows the  $F_a$  values of the LCE and PRx-LCE adhesives at various contact times, and representative photographs taken during the probe tack test. While the  $F_a$  of both samples increased with longer contact times, PRx-LCE exhibited a higher  $F_a$  and more pronounced fibrillation compared to LCE (Figure 5e; Figure S17 and Video S5, Supporting Information). In contrast, PRx-BADA exhibited a lower time-dependent adhesion force and a lower  $F_a$  compared to both LCE and PRx-LCE (Figure 5d,e).

To better understand these results, the contact area was measured as a function of contact time using a Jiusion Digital Microscope. The contact area of PRx-LCE gradually increased with longer contact times ( $10$ – $1800$  s),<sup>[42]</sup> whereas that of LCE saturated at  $600$  s (Figure 5f). This difference may stem from the sliding behavior of PRx in LCE. Creep recovery and stress relaxation experiments were performed to investigate the effect of the sliding motion on the contact area. PRx-LCE showed a higher creep strain ( $\approx 280\%$ ) compared to LCE ( $\approx 110\%$ ) and PRx-BADA ( $\approx 35\%$ ), indicating higher deformability (Figure S18, Supporting Information). Additionally, PRx-LCE exhibited a greater stress relaxation compared to LCE, while maintaining lower residual stress over  $600$  s (Figure S19, Supporting Information). Based on these results, we suggest that the sliding motion of PRx enhances the deformability of PRx-LCE under load during probe tack tests, leading to a larger contact area and deeper indentation, as illustrated in Figure 5f. The  $W_a$  values over contact time, calculated from the probe tack test and contact area, are shown in Figure 5g. Interestingly, the  $W_a$  of PRx-LCE gradually increased, reaching  $1471$  J m $^{-2}$  at a contact time of  $1800$  s, which is a much higher value than the value ( $156$  J m $^{-2}$ ) of LCE at the same contact time. The higher adhesion energy of PRx-LCE compared to that

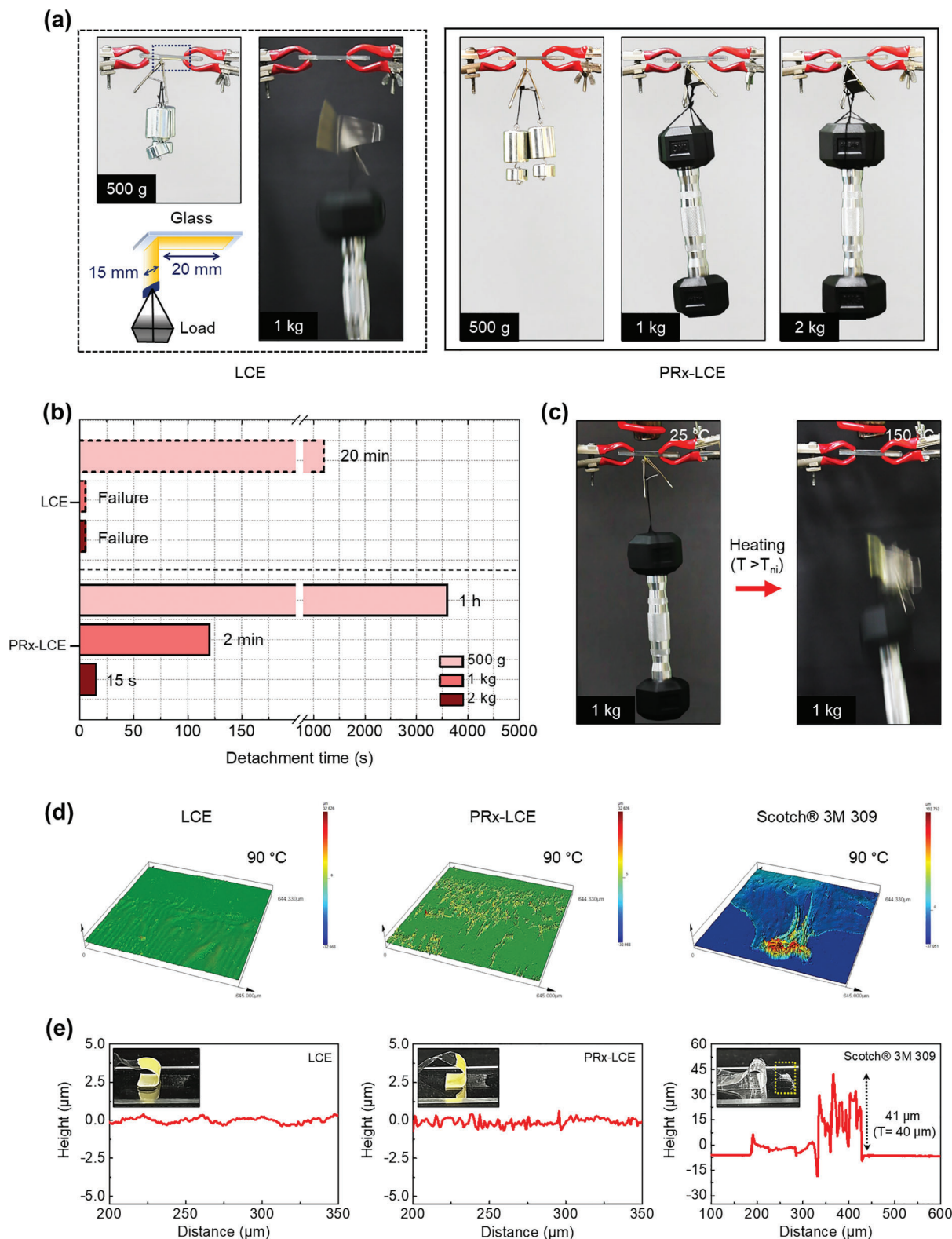


**Figure 4.** a) Comparison of the adhesion strengths between LCE and PRx-LCE adhesives. b) Sustainable load and holding time of LCE and PRx-LCE adhesives. c) Photographs describing the thermally switchable adhesion of PRx-LCE adhesive: the PRx-LCE supports 1 kg, which is released upon heating ( $T > T_{ni}$ ). d) 2D optical images and e) height profiles, obtained using a laser scanning confocal microscope. Inset images are the snapshots during peeling each PSA on the glass substrates.



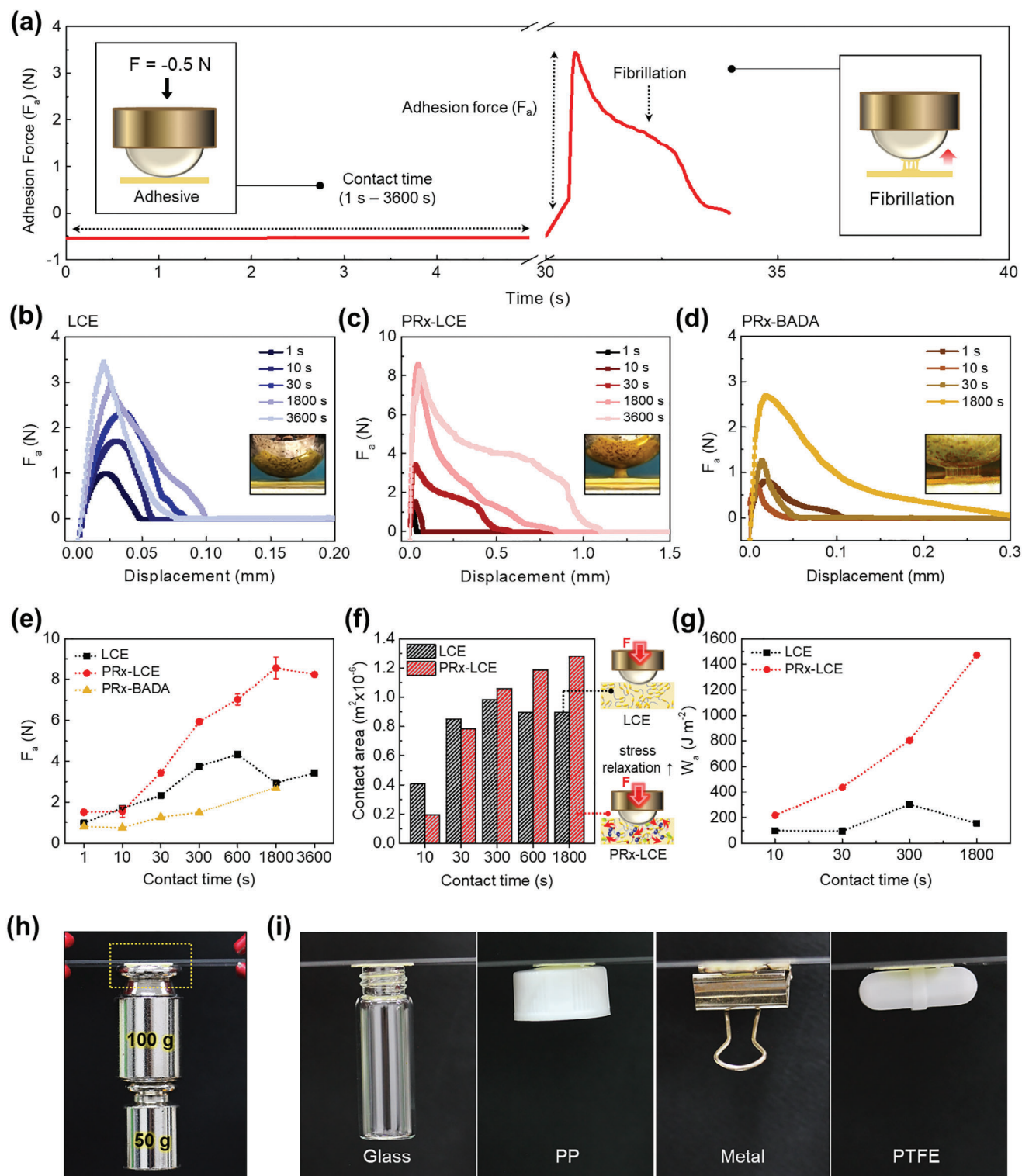


**Figure 5.** a) Schematic of the probe-tack test and adhesion force-time curves. The adhesion force ( $F_a$ ) of b) LCE, c) PRx-LCE, and d) PRx-BADA was measured after various contact times at room temperature. e) A summarized graph that compares the adhesion force of the three PSAs as a function of contact times. f) Contact area of LCE and PRx-LCE adhesives after different contact times (left), and the illustration of stress relaxation behavior of LCE and PRx-LCE adhesives during indentation (right). g) Comparison of the work of adhesion ( $W_a$ ) between LCE and PRx-LCE adhesives after various contact times. h) A photograph of the PRx-LCE adhesive supporting a load of 150 g. i) Adhesion of PRx-LCE to various surfaces, including glass, polypropylene, metal, and polytetrafluoroethylene.



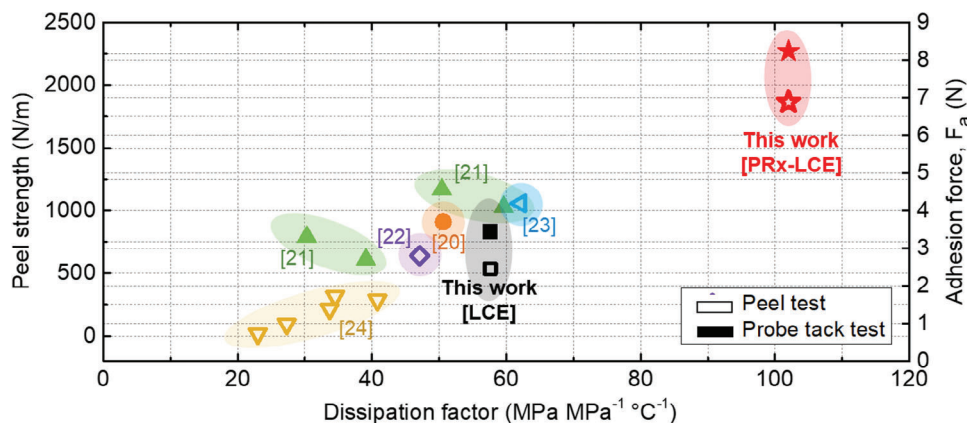


**Figure 6.** Peel strength (from the peel test) and adhesion force (from the probe tack test) over the dissipation factor (area of  $\tan \delta$ ): LCE and PRx-LCE adhesives in this work, and other LCE adhesives reported from literature.<sup>[20–24]</sup>

of LCE is also attributed to the presence of movable crosslinker, which enhances energy dissipation through their sliding motion.

To demonstrate surface adhesion properties, the PRx-LCE adhesive was bonded to a glass cell using glue. Various objects were then attached to the surface of the PRx-LCE adhesive by manually applying gentle pressure. The PRx-LCE adhesive successfully held two steel weights of 50 and 100 g, as shown in Figure 5h, indicating its robust adhesion. Furthermore, the PRx-LCE adhesive exhibited excellent macroscopic adhesion to a range of substrates, including glass, polypropylene (PP), metal, and polytetrafluoroethylene (PTFE), highlighting its versatility and potential for diverse applications (Figure 5i).

### 2.5. Relationship Between Viscoelastic Properties and Adhesion

The adhesion strength is strongly affected by its viscoelastic properties.<sup>[43,44]</sup> For example, the storage modulus is related to effective adhesion, whereas  $\tan \delta$  is associated with energy dissipation during detachment. Generally, higher  $\tan \delta$  values correlate with greater adhesion strength, highlighting the importance of examining the viscoelastic properties of PSAs.

Based on our peel test and probe tack results, as well as values reported in the literature,<sup>[20–24]</sup> we plotted  $\tan \delta$  values and the adhesion strength of LCE adhesives (Figure 6). The area under the  $\tan \delta$  curve, known as the dissipation factor, was used as the x-axis, while the maximum peel strength and adhesion force were plotted on the double y-axes. All data were replotted using WebPlotDigitizer software based on datasets from the literature.

Interestingly, a general trend was observed, indicating that a higher  $\tan \delta$  area corresponds to higher peel strength and adhesion force. The conventional LCE synthesized in this study exhibited adhesion performance similar to those reported in the literature. However, the PRx-LCE adhesive demonstrated significantly higher peel strength and adhesion force compared to other systems. The superior adhesive performance of PRx-LCE results from its unique energy-dissipating characteristics, arising from the synergy between mesogen rotations and movable polyrotaxane crosslinkers, allowing additional freedom for the mesogen motion. If a larger amount of PRx crosslinkers could be intro-

duced to the LCE matrix without an agglomeration issue, the adhesion strength may be further enhanced.

## 3. Conclusion

In summary, we developed a new class of high-performance PSAs by integrating movable PRx crosslinkers into an LCE matrix. Remarkably, PRx-LCE exhibited significantly enhanced energy dissipation compared to conventional LCE, with a more pronounced secondary  $\tan \delta$  peak than that of the primary segmental peak associated with  $T_g$ . This phenomenon was observed in viscoelastic measurements as a function of temperature and frequency. To our knowledge, such unprecedented enhancement in mechanical dissipation has not been reported for LCE systems. The 180° peel test revealed that the peel strength of PRx-LCE was 3.5 times higher than that of conventional LCE and up to 13 times higher than that of commercial PSAs. In addition, the adhesion of PRx-LCE can be switched off when heated close to  $T_{ni}$  without leaving much residue, and then seamlessly recovered when cooled back to the nematic phase. The sliding effect in PRx-LCE also facilitated stress relaxation, resulting in superior adhesion in the probe tack test compared to conventional LCE and commercial PSAs. Our work suggests that integrating mobile moieties, such as the reorientation of mesogens and slidable polyrotaxane crosslinkers, into polymers is an effective strategy for leveraging the dynamic viscoelastic properties of PSAs, thereby enhancing adhesion performance.

## 4. Experimental Section

**Materials:** 1,4-bis-[4-(6-acryloyloxyhexyloxy)benzoyloxy]-2-methylbenzene (RM82) was purchased from Daken Chemical, and bisphenol A ethoxylate diacrylate (BADA) and *n*-butylamine (*n*-BA) were obtained from Sigma-Aldrich. Irgacure-369 (I-369) was donated by the BASF corporation. The polyrotaxane (PRx) cross-linker was synthesized according to a previously established protocol.<sup>[28]</sup> All materials were used without further purification.

**Preparation of PSAs:** The LCE and PRx-LCE adhesives were synthesized by chain-extending the LC monomer (RM82) and *n*-BA through an aza-Michael addition reaction, followed by crosslinking photopolymerization of diacrylate.<sup>[28]</sup> The RM82 to *n*-BA molar ratio was set to 1.1:1, and the weight percentage of I-369 was maintained at 2.5 wt.% of the total LC

mixture. RM82 (10 g, 14.86 mmol), *n*-BA (0.988 g, 13.51 mmol), and I-369 (0.281 g) were added to a vial, and homogeneously mixed using a heat gun. Subsequently, the LC mixture was oligomerized in a convection oven at 80 °C for 21 h. To prepare the PRx-LC oligomer, the LC oligomer was uniformly mixed with a PRx (0.055 g) solution dissolved in chloroform (10 mL) under heating using a heat gun. The weight percentage of the PRx crosslinker was fixed at 0.5 wt.% of the LC oligomer. The PRx-LC oligomer solution was then cast onto a Petri dish and dried in a vacuum oven at 80 °C for 6 h to remove the solvent.

To fabricate the PSA, the LC oligomer was cast onto a PET backing film using a tape-casting coater (MSK-AFA-III, MTI Corporation). Prior to coating, the PET film was treated with O<sub>2</sub> plasma using a plasma cleaner (Diener Plasma GmbH & Co. KG) to ensure a strong bond with the LC oligomer. During the coating process, an applicator with a 500-μm gap was used, moving at a speed of 5 mm s<sup>-1</sup> at 90 °C. Then, the coated LC oligomer was exposed to UV light for 20 min at room temperature for crosslinking. The final thickness of the adhesive was 200 μm. The PRx-BADA adhesive was prepared following the same procedure using BADA (10 g, 19.53 mmol), *n*-BA (1.298 g, 17.75 mmol), and I-369 (0.289 g).

**Material Characterization:** Differential scanning calorimetry (DSC) analysis was performed using a Discovery DSC25 (TA Instruments) under a nitrogen flow. The samples underwent a heating-cooling-heating protocol: first heated to 150 °C, cooled to -50 °C, and then reheated to 150 °C at a rate of 10 °C min<sup>-1</sup>. Viscoelastic measurements as a function of temperature and frequency, creep recovery, and stress relaxation experiments were conducted using a dynamic mechanical analyzer (DMA Q850, TA Instruments) equipped with a tensile clamp. Prior to these tests, the PET film was removed by applying heat, and the samples were cut into rectangular films (7.0 mm (L) × 5.0 mm (W) × 0.2 mm (T)). The temperature ramp for viscoelastic measurements ranged from -50 to 150 °C at a rate of 3 °C min<sup>-1</sup> under a constant frequency of 1 Hz. The frequency sweep test covered a frequency range from 0.1 to 100 Hz and a temperature range from -20 to 120 °C. To generate master curves, TTS was applied with a reference temperature of 20 °C. The creep recovery test was performed at room temperature under constant stress. Each sample was subjected to a constant force of 0.1 N for 30 min, during which the creep strain was monitored over time. After that, the force was removed, and the sample was allowed to recover for an additional 30 min. For the stress relaxation measurements, each sample was subjected to a constant strain of 5%, and the stress relaxation was monitored over time. All samples were equilibrated at 25 °C for 5 min before testing.

**180° Peel Test:** The peel test was performed using a DMA (Q850, TA Instruments) in tensile mode. Adhesives adhered to a PET backing film were mounted onto a stainless-steel substrate, with the steel substrate secured to the top-fixed clamp. Then, the bottom-moving clamp was peeled at a constant rate of 100 mm min<sup>-1</sup>. Peel force measurements were normalized to the adhesive width (10 mm). To investigate the temperature dependency of the adhesives, peel forces were recorded at temperatures ranging from -40 to 100 °C. Prior to testing, all samples were equilibrated at each measurement temperature for 5 min.

**Contact Angle Measurement:** The static contact angle was determined using a contact angle analyzer (Phoenix 300, S.E.O. Co., Ltd., South Korea). The contact angle was measured 10 s after dropping ethylene glycol onto the surface of the adhesives. Measurements were repeated five times at both 20 and 110 °C, with the temperature maintained using a heating pad and monitored by an infrared camera (FLIR, E5-XT).

**Probe Tack Test:** Surface adhesion was measured using a probe tack test, following ASTM D4541 standard. Adhesion forces (*F*<sub>a</sub>) were measured at various contact times using a universal testing machine (ST1 tensiometer, Tinius-Olsen). To ensure precise alignment between the adhesive and probe, a spherical stainless-steel probe with a diameter of 10 mm was employed. The probe moved downward at a rate of 10 mm min<sup>-1</sup>, generating a constant compressive load of 0.5 N. During the test, the probe maintained contact with the adhesive for durations ranging from 1 to 3600 s. Following each contact period, the probe retracted at the same rate until complete separation from the adhesive was achieved. Contact areas at different contact times were measured using a Jiusion digital microscope.

**Residual Analysis:** Microscale residual analysis was conducted using a laser scanning confocal microscope (OLS5000, Olympus). Both LCE and PRx-LCE adhesives were attached to a glass substrate through an annealing process and subsequently peeled off at 90 °C at a constant rate of 100 mm min<sup>-1</sup> using a DMA tensile clamp. Similarly, 3 M tape was applied to the glass substrate and allowed to rest at room temperature for 10 min before being peeled off at 90 °C at the same rate using the DMA tensile clamp. After peeling, the residual surfaces were analyzed using 2D optical images and height profiles obtained from the confocal microscope.

## Supporting Information

Supporting Information is available from the Wiley Online Library or from the author.

## Acknowledgements

This work was supported by the 2022 BK21 FOUR Program of Pusan National University and the National Research Foundation of Korea (NRF) grants funded by the Ministry of Science and ICT (MSIT) of the Korean Government (RS-2023-00208130 and RS-2024-00408845). MS acknowledges the support from the Royal Society through University Research Fellowships (Grant Number: G113670).

## Conflict of Interest

The authors declare no conflict of interest.

## Data Availability Statement

The data that support the findings of this study are available from the corresponding author upon reasonable request.

## Keywords

adhesion, damping, liquid crystal elastomers, polyrotaxanes, pressure sensitive adhesives

Received: July 31, 2024

Revised: October 25, 2024

Published online: November 13, 2024

- [1] T. H. Ware, M. E. McConney, J. J. Wie, V. P. Tondiglia, T. J. White, *Science* **2015**, *347*, 982.
- [2] J. Lee, Y. Guo, Y.-J. Choi, S. Jung, D. Seol, S. Choi, J.-H. Kim, Y. Kim, K.-U. Jeong, S.-k. Ahn, *Soft Matter* **2020**, *16*, 2695.
- [3] K. Kim, Y. Guo, J. Bae, S. Choi, H. Y. Song, S. Park, K. Hyun, S.-k. Ahn, *Small* **2021**, *17*, 2100910.
- [4] T. Guin, M. J. Settle, B. A. Kowalski, A. D. Augustine, R. V. Beblo, G. W. Reich, T. J. White, *Nat. Commun.* **2018**, *9*, 2531.
- [5] Q. He, Z. Wang, Y. Wang, Z. Wang, C. Li, R. Annapooranan, J. Zeng, R. Chen, S. Cai, *Sci. Robot.* **2021**, *6*, eabi9704.
- [6] Y. J. Lee, M. K. Abdelrahman, M. S. Kalairaj, T. H. Ware, *Small* **2023**, *19*, 2302774.
- [7] M. Camacho-Lopez, H. Finkelmann, P. Palffy-Muhoray, M. Shelley, *Nat. Mater.* **2004**, *3*, 307.
- [8] X. Peng, S. Wu, X. Sun, L. Yue, S. M. Montgomery, F. Demoly, K. Zhou, R. R. Zhao, H. J. Qi, *Adv. Mater.* **2022**, *34*, 2204890.

- [9] J.-H. Lee, J. Bae, J. H. Hwang, M.-Y. Choi, Y. S. Kim, S. Park, J.-H. Na, D.-G. Kim, S.-k. Ahn, *Adv. Funct. Mater.* **2022**, 32, 2110360.
- [10] I. H. Kim, S. Choi, J. Lee, J. Jung, J. Yeo, J. T. Kim, S. Ryu, S.-k. Ahn, J. Kang, P. Poulin, S. O. Kim, *Nat. Nanotechnol.* **2022**, 17, 1198.
- [11] D. Martella, C. Parmeggiani, Zeng, *Chem. Eur. J.* **2018**, 24, 12206.
- [12] D. Mistry, N. A. Traugutt, B. Sanborn, R. H. Volpe, L. S. Chatham, R. Zhou, B. Song, K. Yu, K. N. Long, C. M. Yakacki, *Nat. Commun.* **2021**, 12, 6677.
- [13] S. Y. Jeon, B. Shen, N. A. Traugutt, Z. Zhu, L. Fang, C. M. Yakacki, T. D. Nguyen, S. H. Kang, *Adv. Mater.* **2022**, 34, 2200272.
- [14] C. Luo, C. Chung, N. A. Traugutt, C. M. Yakacki, K. N. Long, K. Yu, *ACS Appl. Mater. Interfaces* **2021**, 13, 12698.
- [15] M. O. Saed, W. Elmadih, A. Terentjev, D. Chronopoulos, D. Williamson, E. M. Terentjev, *Nat. Commun.* **2021**, 12, 6676.
- [16] S. M. Clarke, A. R. Tajbakhsh, E. M. Terentjev, C. Remillat, G. R. Tomlinson, J. R. House, *J. Appl. Phys.* **2001**, 89, 6530.
- [17] S. M. Clarke, A. R. Tajbakhsh, E. M. Terentjev, M. Warner, *Phys. Rev. Lett.* **2001**, 86, 4044.
- [18] N. A. Traugutt, R. H. Volpe, M. S. Bollinger, M. O. Saed, A. H. Torbati, K. Yu, N. Dadivanyan, C. M. Yakacki, *Soft Matter* **2017**, 13, 7013.
- [19] D. R. Corbett, J. M. Adams, *Soft Matter* **2013**, 9, 1151.
- [20] T. Ohzono, M. O. Saed, E. M. Terentjev, *Adv. Mater.* **2019**, 31, 1902642.
- [21] H. J. Farre-Kaga, M. O. Saed, E. M. Terentjev, *Adv. Funct. Mater.* **2022**, 32, 2110190.
- [22] H. Guo, M. O. Saed, E. M. Terentjev, *Macromolecules* **2023**, 56, 6247.
- [23] R. Annapooranan, S. S. Jeyakumar, R. J. Chambers, R. Long, S. Cai, *Adv. Funct. Mater.* **2024**, 34, 2309123.
- [24] P. A. Pranda, A. Hedegaard, H. Kim, J. Clapper, E. Nelson, L. Hines, R. C. Hayward, T. J. White, *ACS Appl. Mater. Interfaces* **2024**, 16, 6394.
- [25] K. Ito, *Polym. J.* **2012**, 44, 38.
- [26] M.-B. Yi, T.-H. Lee, G.-Y. Han, H. Kim, H.-J. Kim, Y. Kim, H.-S. Ryou, D.-U. Jin, *ACS Appl. Polym. Mater.* **2021**, 3, 2678.
- [27] K. V. Dikshit, A. M. Visal, F. Janssen, A. Larsen, C. J. Bruns, *ACS Appl. Mater. Interfaces* **2023**, 15, 17256.
- [28] S. Choi, B. Kim, S. Park, J.-H. Seo, S.-k. Ahn, *ACS Appl. Mater. Interfaces* **2022**, 14, 32486.
- [29] S. Disch, C. Schmidt, H. Finkelmann, *Macromol. Rapid Commun.* **1994**, 15, 303.
- [30] M. O. Saed, C. P. Ambulo, H. Kim, R. De, V. Raval, K. Searles, D. A. Siddiqui, J. M. O. Cue, M. C. Stefan, M. R. Shankar, T. H. Ware, *Adv. Funct. Mater.* **2019**, 29, 1806412.
- [31] X.-S. Wang, H.-K. Kim, Y. Fujita, A. Sudo, H. Nishida, T. Endo, *Macromolecules* **2006**, 39, 1046.
- [32] A. Hanafusa, S. Ando, S. Ozawa, M. Ito, R. Hasegawa, K. Mayumi, K. Ito, *Polym. J.* **2020**, 52, 1211.
- [33] S. Pruksawan, S. Samitsu, H. Yokoyama, M. Naito, *Macromolecules* **2019**, 52, 2464.
- [34] J. D. Ferry, *Viscoelastic Properties of Polymers*, John Wiley & Sons, New York, US **1980**.
- [35] A. Hotta, E. M. Terentjev, *Eur. Phys. J. E.* **2003**, 10, 291.
- [36] S. Sun, M. Li, A. Liu, *Int. J. Adhes. Adhes.* **2013**, 41, 98.
- [37] P. Ananthasubramanian, R. Sahay, N. Raghavan, *Sci. Rep.* **2024**, 14, 4487.
- [38] M. D. Bartlett, S. W. Case, A. J. Kinloch, D. A. Dillard, *Prog. Mater. Sci.* **2023**, 137, 101086.
- [39] S. D. Roy, M. Gutierrez, G. L. Flynn, G. W. Cleary, *J. Pharm. Sci.* **1996**, 85, 491.
- [40] J. Hwang, D. Lim, G. Lee, Y. E. Kim, J. Park, M.-J. Baek, H.-S. Kim, K. Park, K. H. Ku, D. W. Lee, *Mater. Horiz.* **2023**, 10, 2013.
- [41] C.-H. Park, S.-J. Lee, T.-H. Lee, H.-J. Kim, *React. Funct. Polym.* **2016**, 100, 130.
- [42] A. Maghsoodi, M. O. Saed, E. M. Terentjev, K. Bhattacharya, *Extreme Mech. Lett.* **2023**, 63, 102060.
- [43] C. Creton, *MRS Bull.* **2003**, 28, 434.
- [44] C. Creton, M. Ciccotti, *Rep. Prog. Phys.* **2016**, 79, 046601.